


## Article

# Lithium Enrichment by the Carbothermal Reduction of Spodumene Ore and the Preparation of Manganese-Silicon Alloy

Mingliang Yang <sup>1,2,3</sup> , Ke Yan <sup>1,2,3</sup>, Rui Ji <sup>1,2,3</sup>, Xi Cui <sup>1,2,3</sup>, Wenzheng Zhang <sup>1,2,3</sup> and Tao Qu <sup>1,2,3,4,\*</sup>

<sup>1</sup> Faculty of Metallurgical and Energy Engineering, Kunming University of Science and Technology, Kunming 650093, China

<sup>2</sup> National Engineering Research Center of Vacuum Metallurgy State, Kunming University of Science and Technology, Kunming 650093, China

<sup>3</sup> Key Laboratory for Nonferrous Vacuum Metallurgy of Yunnan Province, Kunming University of Science and Technology, Kunming 650093, China

<sup>4</sup> State Key Laboratory of Complex Nonferrous Metals Resources Clear Utilization, Kunming University of Science and Technology, Kunming 650093, China

\* Correspondence: qutao\_82@126.com; Tel.: +86-13518715200

**Abstract:** To increase the low utilization rate of spodumene ore during lithium extraction, spodumene ore was subjected to carbothermic reduction to enrich lithium and prepare a manganese-silicon alloy. The experimental results showed that during thermal reduction, lithium was volatilized and collected in the condensation zone. The Li<sub>2</sub>O content in the lithium condensate was 41.72%, which was 10.85 times higher than that of the raw material. The effects of varying reduction temperatures and times on the lithium volatilization rate and direct yield of Mn<sub>5</sub>Si<sub>3</sub> alloy were investigated. The best process conditions were 1873 K for 6 h. Under these conditions, the lithium volatilization rate was 97.65%, and the direct yield of Mn<sub>5</sub>Si<sub>3</sub> was 86.47%.

**Keywords:** spodumene ore; lithium enrichment; manganese silicon alloy



**Citation:** Yang, M.; Yan, K.; Ji, R.; Cui, X.; Zhang, W.; Qu, T. Lithium Enrichment by the Carbothermal Reduction of Spodumene Ore and the Preparation of Manganese-Silicon Alloy. *Minerals* **2022**, *12*, 1324. <https://doi.org/10.3390/min12101324>

Academic Editor: Rajesh Kumar Jyothi

Received: 26 September 2022

Accepted: 17 October 2022

Published: 20 October 2022

**Publisher's Note:** MDPI stays neutral with regard to jurisdictional claims in published maps and institutional affiliations.



**Copyright:** © 2022 by the authors. Licensee MDPI, Basel, Switzerland. This article is an open access article distributed under the terms and conditions of the Creative Commons Attribution (CC BY) license (<https://creativecommons.org/licenses/by/4.0/>).

## 1. Introduction

With the rapid development of science and technology, lithium is an important material for nuclear energy, energy storage, aerospace, and other fields [1–4]. Lithium extraction from spodumene ore is an important process in the production of lithium products [5–7]. As an aluminosilicate ore [8–10], the theoretical composition of spodumene is 8.03% Li<sub>2</sub>O [11,12], 27.4% Al<sub>2</sub>O<sub>3</sub>, and 64.6% SiO<sub>2</sub> [13]. Lithium extraction from spodumene ore is still mainly performed by the sulfuric acid method [14–17]. When lithium is extracted by the sulfuric acid method, the spodumene ore is transformed and roasted at 900–1050 °C, and the dense  $\alpha$ -spodumene ( $\alpha$ -LiAlSi<sub>2</sub>O<sub>6</sub>) is transformed into loose  $\beta$ -spodumene ( $\beta$ -LiAlSi<sub>2</sub>O<sub>6</sub>).  $\beta$ -LiAlSi<sub>2</sub>O<sub>6</sub> is mixed with excess concentrated sulfuric acid and subjected to secondary calcination at 170–250 °C. The calcined product is concentrated, immersed in water, and filtered to obtain purified Li<sub>2</sub>SO<sub>4</sub> concentrate. Then, Na<sub>2</sub>CO<sub>3</sub> is added to the concentrate to undergo ion exchange with Li<sub>2</sub>SO<sub>4</sub> to obtain insoluble Li<sub>2</sub>CO<sub>3</sub> precipitate [18–21]. The sulfuric acid method only considers the extraction of Li and converts Si<sub>2</sub>O and Al<sub>2</sub>O<sub>3</sub> in spodumene ore into hazardous waste residues [22,23]. Taking spodumene concentrate with 6% Li<sub>2</sub>O content as an example, for every ton of lithium carbonate (Li<sub>2</sub>CO<sub>3</sub>) that is produced, 8–10 tons of hazardous waste slag and 6–9 tons of high-salt wastewater are produced [24–26]. This causes environmental pollution and wastes resources.

Owing to the problems associated with the acid-sulfur method, in this paper, lithium was enriched by adding coke and manganese dioxide (MnO<sub>2</sub>) to spodumene by thermal reduction. SiO<sub>2</sub> and Al<sub>2</sub>O<sub>3</sub> were recovered in spodumene ore. The reported method

represents a new technology for lithium extraction from spodumene for the comprehensive recovery and utilization of its valuable components.

## 2. Materials and Methods

### 2.1. Materials

The spodumene ore used in the experiment was obtained from Africa. X-ray diffraction was used to analyze the crystal phases of spodumene; the results are shown in Figure 1. The ore was composed of spodumene ( $\text{LiAlSi}_2\text{O}_6$ ) and quartz ( $\text{SiO}_2$ ). Inductively coupled plasma emission spectroscopy (ICP-OES) was used for quantitative element analysis of the ore; the results are shown in Table 1. The coke was produced by Ningxia Huiheng (China), and its composition is shown in Table 2.

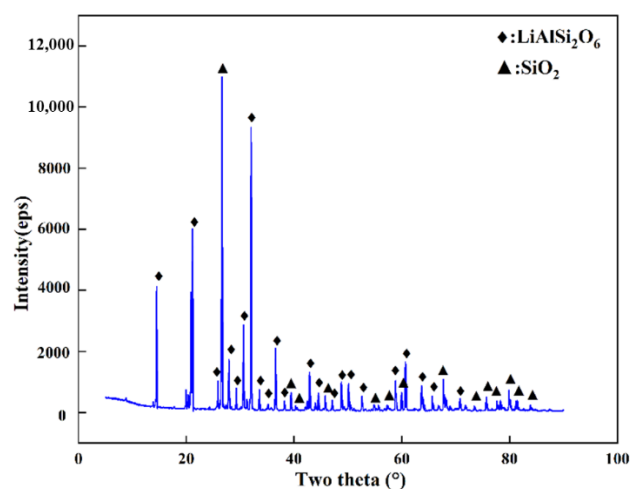


Figure 1. XRD pattern of spodumene ore.

Table 1. Spodumene ore composition.

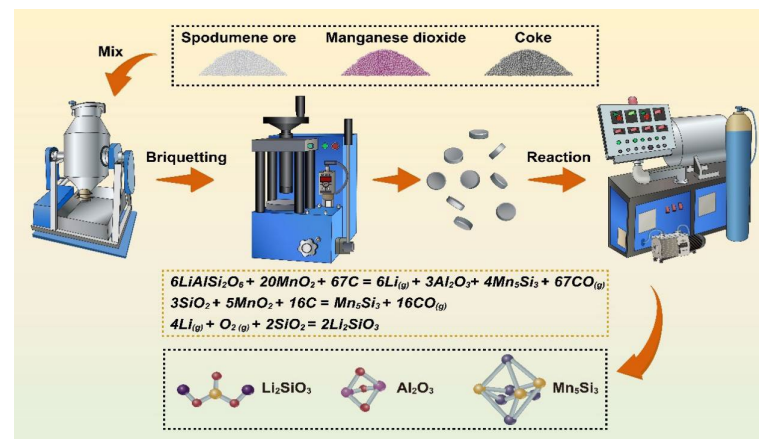
Component	$\text{SiO}_2$	$\text{Al}_2\text{O}_3$	$\text{Li}_2\text{O}$	$\text{Fe}_2\text{O}_3$	$\text{Na}_2\text{O}$	$\text{K}_2\text{O}$	$\text{CaO}$	Other
Content(wt.%)	72.50	18.60	3.84	0.94	0.36	0.62	0.01	3.13

Table 2. Coke composition.

Component	Ash	Volatile	Moisture	Solid Carbon
Content (wt.%)	11.64	1.54	0.5	86.32

### 2.2. Methods

First, the spodumene ore and coke were crushed and screened through 200 mesh. The spodumene ore, coke, and manganese dioxide were mixed evenly ( $w_{\text{LiAlSi}_2\text{O}_6} : w_{\text{MnO}_2} : w_{\text{C}} = 5 : 5 : 4$ ), pressed into blocks under a pressure of 18 MPa, and placed into the graphite crucible of a vacuum furnace. The vacuum pump was turned on, and after reaching the vacuum state, argon gas was passed until the pressure reached  $3 \times 10^4$ – $3.5 \times 10^4$  Pa (the atmospheric pressure in the experimental area was about  $8 \times 10^4$  Pa). Heating was started according to the preset experimental conditions at a rate of approximately 10 K/min. At the end of the reaction (the pressure in the furnace was about  $7 \times 10^4$ – $7.5 \times 10^4$  Pa), the residue in the graphite crucible and the condensate in the stainless-steel crucible were removed for characterization. The reaction process flow was shown in Figure 2.



**Figure 2.** Schematic diagram of the reaction process. The raw materials were first mixed by a blender; then, the mixture was pressed into a round cake shape, entering the vacuum furnace for the preset experimental conditions.

### 2.3. Characterization Methods

#### 2.3.1. Lithium Volatilization Rate

In the formula,  $\partial_{\text{Li}}$  is the volatilization rate of lithium,  $m_{\text{Li}}$  is the mass of lithium in the reduced residue, and  $M_{\text{Li}}$  is the mass of lithium in the raw material.

$$\partial_{\text{Li}} = \left(1 - \frac{m_{\text{Li}}}{M_{\text{Li}}}\right) \times 100\% \quad (1)$$

#### 2.3.2. Lithium Enrichment Rate

In the formula,  $\gamma_{\text{Li}}$  is the enrichment ratio of lithium,  $w_{\text{Li}}$  is the content of Li in the condensate, and  $W_{\text{Li}}$  is the content of Li in the raw material.

$$\gamma_{\text{Li}} = \left(1 - \frac{w_{\text{Li}}}{W_{\text{Li}}}\right) \times 100\% \quad (2)$$

#### 2.3.3. Alloy Direct Yield

In the formula,  $\beta_{\text{Mn}_5\text{Si}_3}$  is the direct yield of manganese-silicon alloy,  $m_{\text{Mn}_5\text{Si}_3}$  is the mass of manganese-silicon alloy in the reduced residue, and  $M_{\text{Mn}_5\text{Si}_3}$  is the mass of manganese-silicon alloy in the raw material.

$$\beta_{\text{Mn}_5\text{Si}_3} = \frac{m_{\text{Mn}_5\text{Si}_3}}{M_{\text{Mn}_5\text{Si}_3}} \times 100\% \quad (3)$$

#### 2.3.4. Testing Equipment

The phases in spodumene, condensate, and reduction products were detected by X-ray diffractometry (XRD, X'Pert Pro MPD, Nalytical, Heracles, Almelo, The Netherlands). Inductively coupled plasma emission spectroscopy (ICP-OES, Optima 8300, PerkinElmer, Waltham, MA, USA) was used to quantitatively analyze the main chemical components in the raw materials. The morphology of the reduced products was observed and characterized by scanning electron microscopy (TM-3030 Plus, Hitachi, Tokyo, Japan) and energy-dispersive spectrometry (INCA, Oxford, UK). The lithium content of the condensate and reduction products was measured by an atomic absorption spectrophotometer (AAS; iCE 3500, Thermo, Waltham, MA, USA).

### 3. Results and Discussion

#### 3.1. Thermodynamic Calculations

HSC6.0 thermodynamic software was used to calculate the possible reactions; the results are shown in Figure 3.  $\text{SiO}_2$  in the ore participated during the reaction and preferentially formed  $\text{LiAlSi}_2\text{O}_6$ , indicating that  $\text{Mn}_5\text{Si}_3$  was preferentially formed over lithium vapor and alumina ( $\text{Al}_2\text{O}_3$ ). When  $\text{MnO}_2$  was added to the reaction, the reaction temperature dropped significantly to 651 K and 667 K lower than that of  $\text{SiO}_2 + \text{C}$  and  $\text{LiAlSi}_2\text{O}_6 + \text{C}$ , respectively, indicating that adding  $\text{MnO}_2$  reduced the reaction temperature and facilitated the reaction. Therefore, this process was thermodynamically feasible.

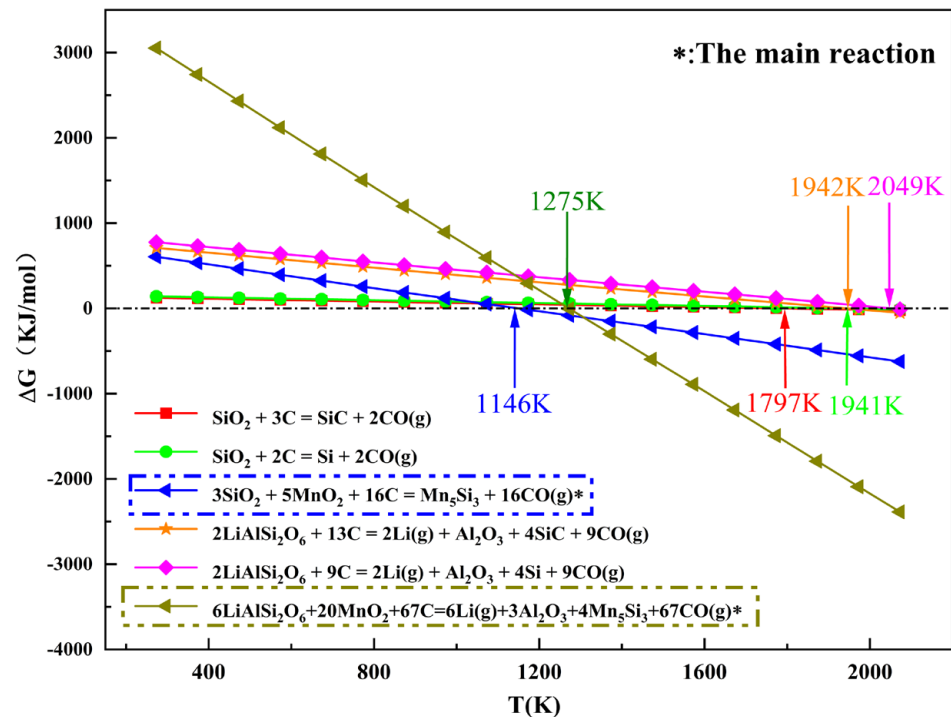


Figure 3. Thermodynamic calculations of possible reactions.

#### 3.2. Condensate Analysis

Due to the limited feed amount and the low lithium content in spodumene ore, it was difficult to collect the lithium condensate in a single step, so the lithium-rich condensate was collected through multiple experiments. The phase analysis of the condensate was carried out by XRD; the results are shown in Figure 4. Li mainly existed in the condensate in the form of  $\text{Li}_2\text{SiO}_3$ . By referring to the literature [27], we found that  $\text{Li}_2\text{O}$  and  $\text{SiO}_2$  formed eutectic compounds in the range of 1028–1201 °C. Therefore, it is believed that the  $\text{Li}_2\text{SiO}_3$  generated in the condensation zone was formed by Li in the condensation zone and  $\text{O}_2$  in air to generate  $\text{Li}_2\text{O}$ , which then reacted with  $\text{SiO}_2$  to form eutectic compounds. The reaction equation is shown in Reaction 4. The Li content in the condensate was 19.47%, as detected by atomic absorption spectrophotometry, and the  $\text{Li}_2\text{O}$  content was 41.72%, which was 10.85 times more enriched compared with spodumene.



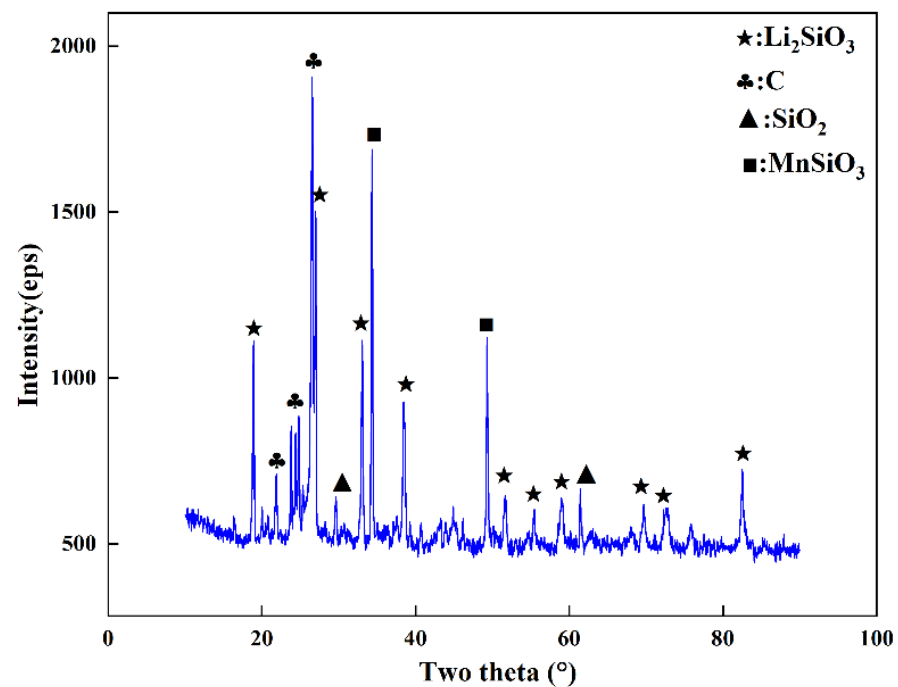


Figure 4. XRD pattern of the condensate.

### 3.3. The Effect of Temperature

Based on the theoretical calculations and experimental exploration, the reduction time was set to 6 h to ensure the completion of the reaction. After the reaction, due to differences in density, the graphite crucible underwent delamination. Figures 5 and 6 show the XRD patterns of the lower- and upper-layer materials from 1673 K to 1973 K with a holding time of 6 h. Figure 5 shows that  $\text{LiAlSi}_2\text{O}_6$  did not begin to react at 1673 K or 1723 K, indicating that the reaction temperature was too low. The  $\text{Mn}_5\text{Si}_3$  diffraction peak appeared because  $\text{SiO}_2$  in the ore preferentially reacted with C and  $\text{MnO}_2$ , which was consistent with the thermodynamic calculations showing that  $\text{SiO}_2$  should preferentially produce  $\text{LiAlSi}_2\text{O}_6$ . However, as shown in Figure 6, SiC and  $\text{Mn}_2\text{C}_5$  were present in the upper-layer material, and SiC and  $\text{Mn}_2\text{C}_5$  were intermediates during the formation of  $\text{Mn}_5\text{Si}_3$ . This indicates that the reaction between  $\text{SiO}_2$  and  $\text{MnO}_2$  was incomplete. When the temperature reached 1773 K and 1823 K, the diffraction peaks shown in Figure 6 all changed to those of  $\text{Mn}_5\text{Si}_3$ , indicating that the lower-layer material was composed of alloys at these temperatures. The diffraction peaks of  $\text{Al}_2\text{O}_3$  and  $\text{LiAlSi}_2\text{O}_6$  shown in Figure 6 indicate that  $\text{LiAlSi}_2\text{O}_6$  began to react but did so incompletely. When the temperature was 1873 K, the diffraction peak of  $\text{LiAlSi}_2\text{O}_6$  shown in Figure 6 disappeared, and the intensity of the diffraction peaks of  $\text{Al}_2\text{O}_3$  and SiC was enhanced. At this time,  $\text{LiAlSi}_2\text{O}_6$  completely reacted, but the diffraction peak of  $\text{Mn}_5\text{Si}_3$  remained, indicating that a small amount of  $\text{Mn}_5\text{Si}_3$  was mixed into the upper-layer material. As the reaction temperature continued to increase, the  $\text{Mn}_5\text{Si}_3$  diffraction peak remained. When the temperature was 1923 K, the intensity of the SiC diffraction peak shown in Figure 6 was enhanced, indicating that the SiC content increased. The high content of SiC affected the viscosity of the upper-layer material, which inhibited the upward diffusion of lithium vapor, resulting in a decrease in the volatilization rate of lithium. Therefore, the formation of SiC should be controlled during the reaction.

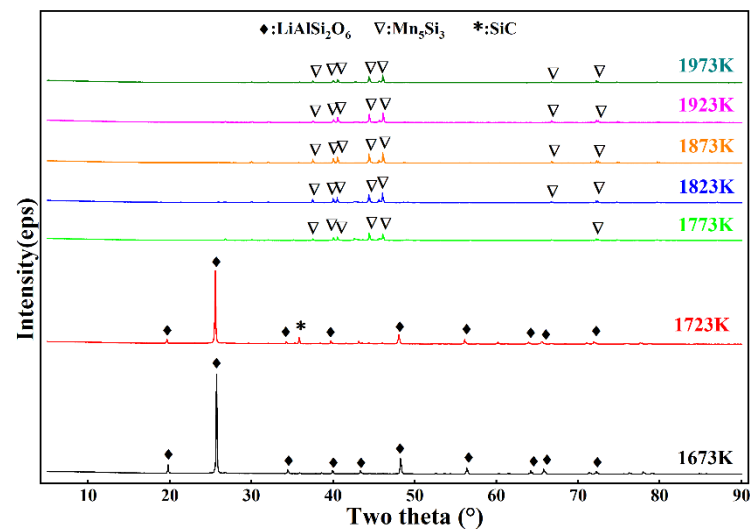


Figure 5. XRD patterns of the underlying material at varying reduction temperatures.

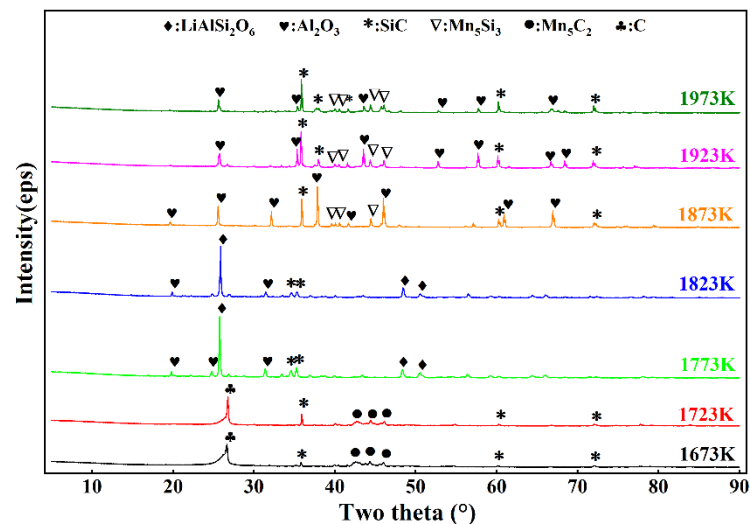


Figure 6. XRD patterns of the upper layer at varying reduction temperatures.

The direct yield of  $Mn_5Si_3$  was obtained by weighing the alloy in the lower-layer material, as shown in Figure 7. The direct yield of  $Mn_5Si_3$  was low at temperatures below 1873 K because the spodumene ore had not completely reacted to form an alloy. When the temperature was 1873 K, the direct yield of  $Mn_5Si_3$  was 86.47%, which was the maximum yield. Continuing to increase the reaction temperature resulted in a slight decrease in the direct yield of  $Mn_5Si_3$ . The reason for the low direct yield of  $Mn_5Si_3$  was that the formation of SiC caused the loss of Si, and a small amount of  $Mn_5Si_3$  entered the upper layer. After grinding and mixing the reduced residues in a graphite crucible at varying reduction temperatures, the Li content was detected by atomic absorption spectrophotometry. The influence of varying reduction temperatures on the volatilization rate of Li during the experimental process was investigated; the results are shown in Figure 8. At temperatures below 1723 K, spodumene ore did not participate in the reaction, so the volatilization rate of lithium was 0%. When the reduction temperature was 1773 K, the volatilization rate of Li was 32.75%, indicating that  $LiAlSi_2O_6$  had begun to be reduced at this temperature, although the reduction degree was low. Upon increasing the temperature, the volatilization rate of Li gradually increased. When the temperature was 1873 K, the volatilization rate of Li was 97.65%. Upon continuing to increase the temperature, the Li volatilization rate remained identical to that at 1873 K, indicating that spodumene completely reacted at 1873 K. This was consistent with the analysis of the results presented in Figures 5 and 6.

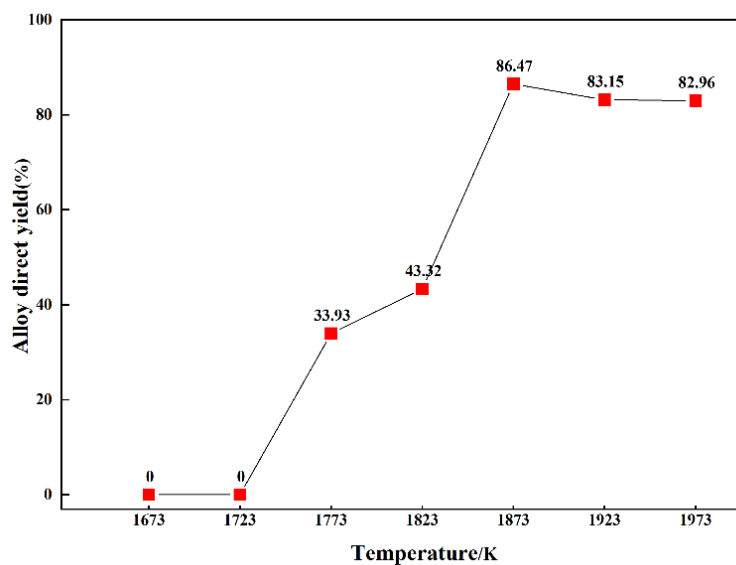


Figure 7. Direct yields of alloys at varying reduction temperatures.

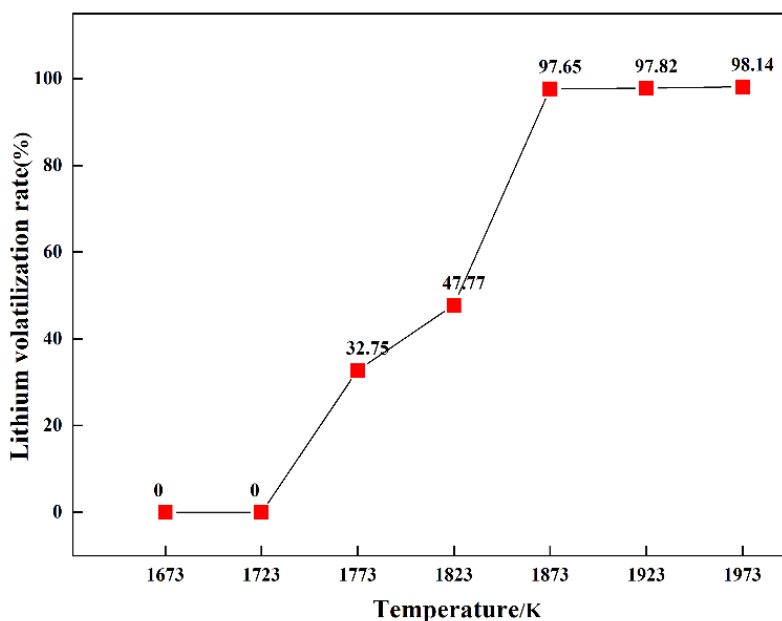


Figure 8. Reduction rates of lithium at varying reaction temperatures.

### 3.4. The Effect of Time

In the previous section, the optimal reduction temperature was determined to be 1873 K by exploring the influence of temperature. In this section, we designed a gradient pair experiment with a reduction time of 1–10 h at the optimal reduction temperature. The material ratio and detection and treatment method used in the experiment were the same as those described in the previous section. Figure 9 shows that before 4 h, in addition to the  $Mn_5Si_3$  diffraction peaks, there were  $Mn_5C_2$  and SiC diffraction peaks in the lower-layer material. These peaks indicate that the reaction was incomplete. Upon increasing the reduction time to 6 h, the diffraction peaks of the lower-layer material were due to  $Mn_5Si_3$  and  $Mn_5C_2$ . The SiC diffraction peaks disappeared, which showed that 6 h was enough to completely separate the upper and lower layers. Figure 10 shows that when the reduction time was 4 h, the diffraction peak of  $LiAlSi_2O_6$  disappeared. Thus,  $LiAlSi_2O_6$  was completely reduced, but  $MnO_2$  was not completely reduced, indicating that  $MnO_2$  required a longer reduction time than  $LiAlSi_2O_6$ .

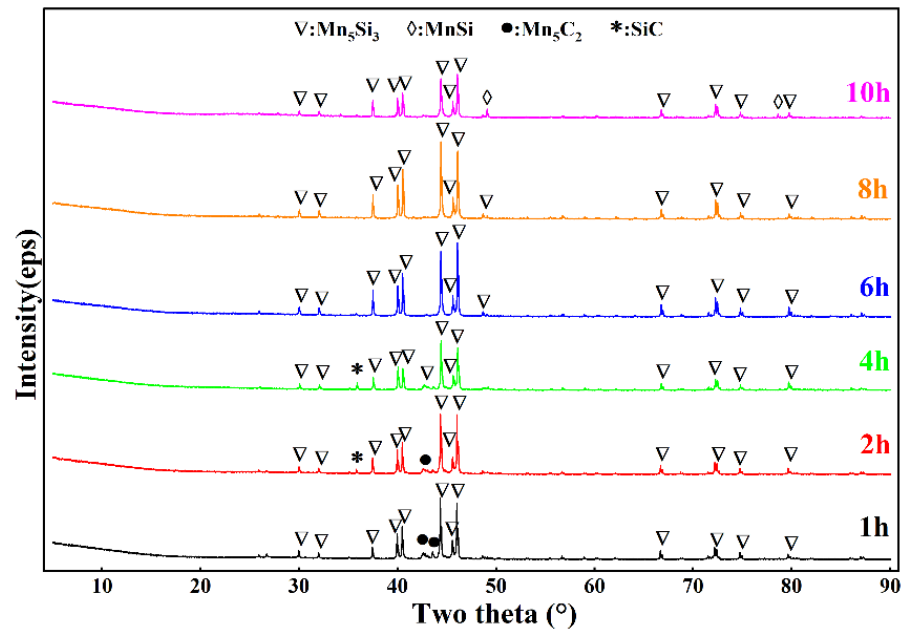


Figure 9. XRD patterns of the middle and lower alloys in the reduction residue with varying holding times.

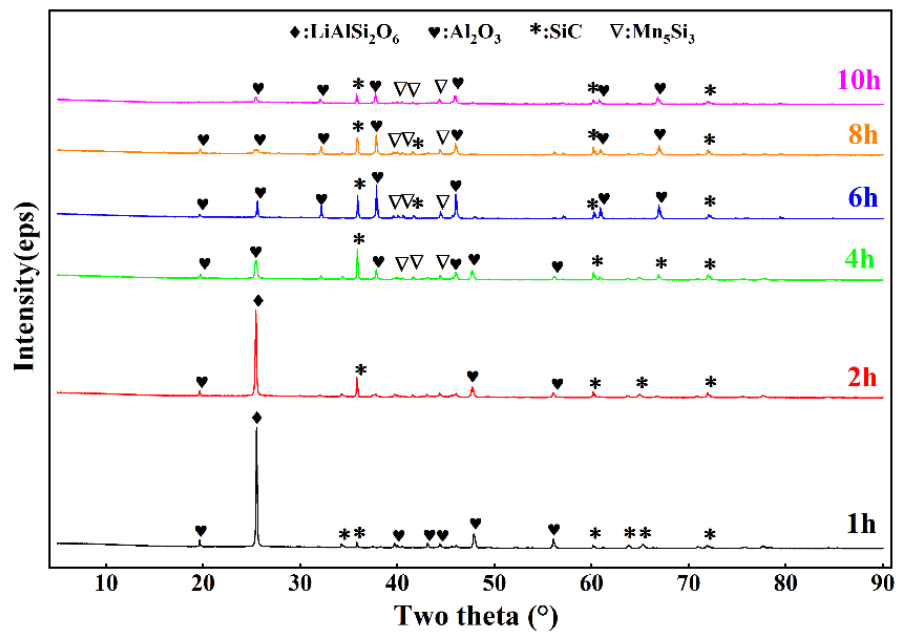


Figure 10. XRD patterns of the upper and middle slag in the reduction residue with varying holding times.

The direct yield of  $Mn_5Si_3$  with varying reduction times is shown in Figure 11. The direct yield of  $Mn_5Si_3$  increased significantly when the reduction time was increased 2 h to 4 h, from 56.33% to 81.55%, indicating that  $LiAlSi_2O_6$  was involved in the reaction from 2 h to 4 h. When the reduction time was 6 h, the direct yield of the alloy was the highest. When the reduction time was increased to 8 h, the direct yield of  $Mn_5Si_3$  decreased slightly, but the change was insignificant.



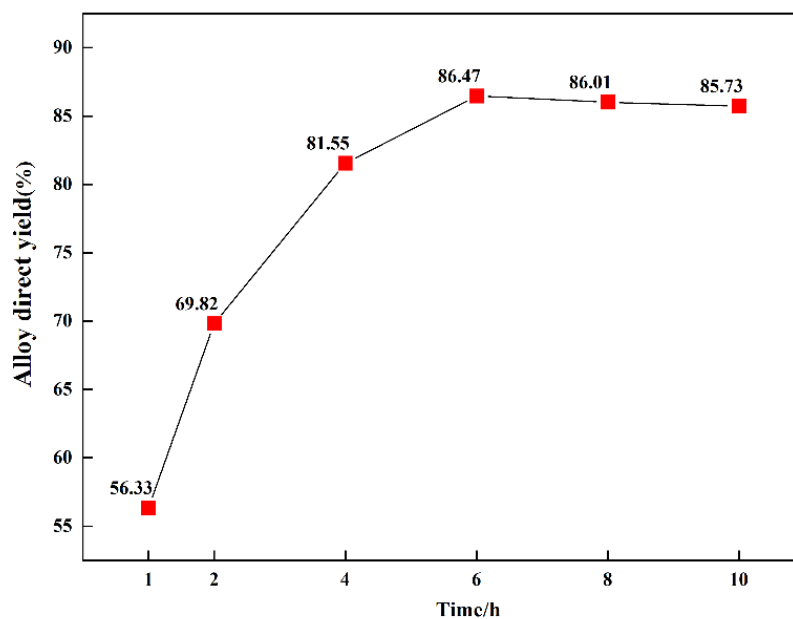


Figure 11. Direct yield of the manganese-silicon alloy with varying holding times.

The volatilization rate of lithium with varying reduction times is shown in Figure 12. There was a large increase in 2–4 h, which further verified the conclusion that  $\text{LiAlSi}_2\text{O}_6$  was considerably reduced with reaction times of 2–4 h. Upon extending the time, the volatilization rate of lithium increased gradually. When the reduction time was 6 h, the volatilization rate of lithium reached 97.65%, and the reduction of lithium was complete.

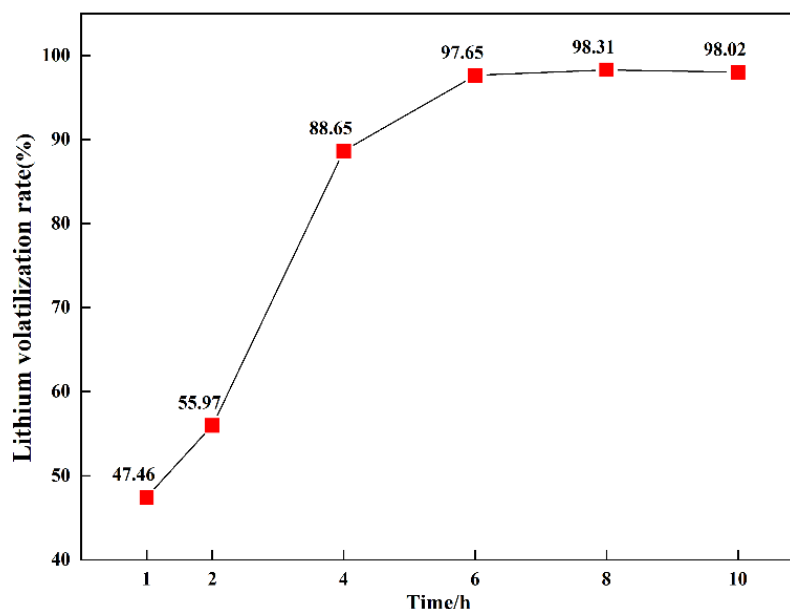


Figure 12. Reduction rates of lithium with varying reduction times.

Based on single-factor experimental analysis, it can be concluded that the optimal parameters for studying lithium enrichment by the carbothermal reduction of spodumene to prepare manganese-silicon alloy were 1873 K and 6 h.

### 3.5. SEM-EDS Analysis

The upper- and lower-layer materials under the abovementioned optimal conditions were analyzed by SEM-EDS; the results are shown in Figures 13 and 14. Figure 13a shows

that the alloy was bright white with a smooth surface and no cracks or other defects. Figure 13b,c shows that the coincidence degree of Mn and Si was high.

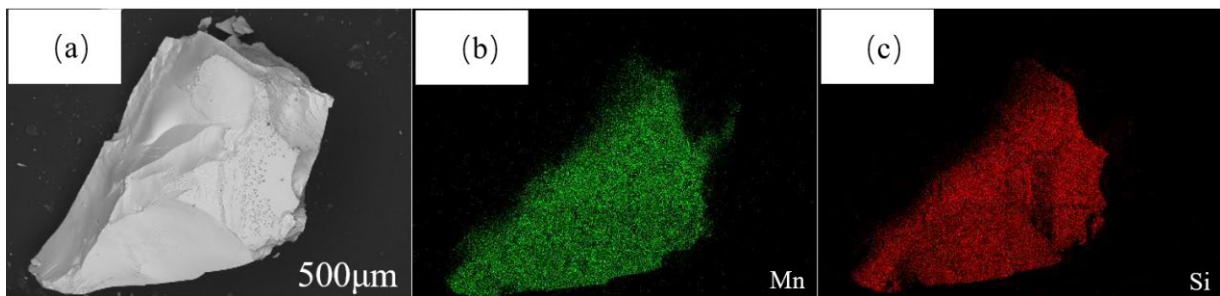


**Figure 13.** SEM-EDS image of the upper layer at 1873 K and 6 h: (a) SEM image; (b) Mn element distribution; (c) Si element distribution.

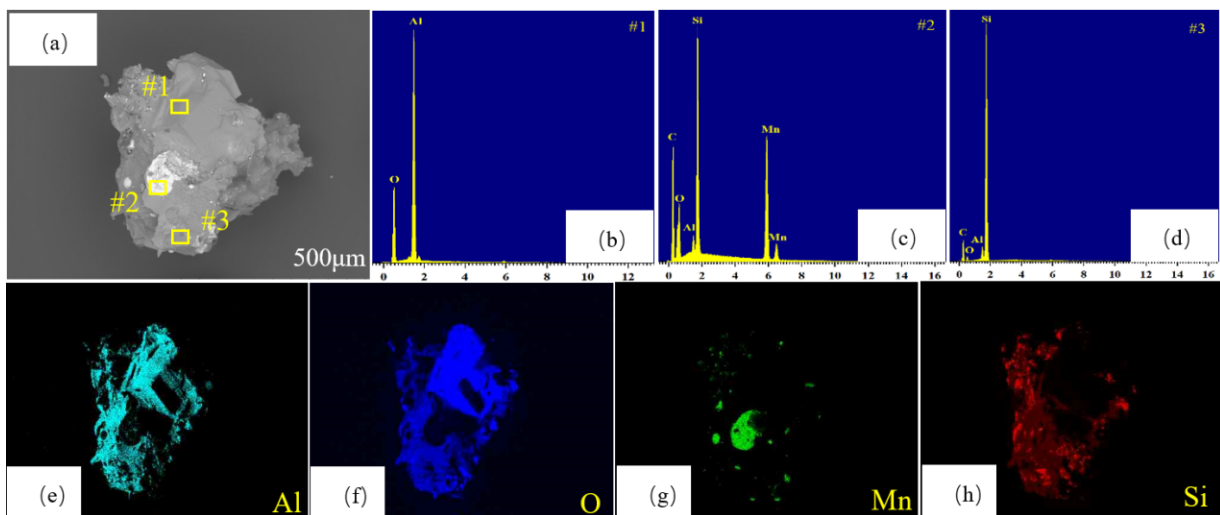


**Figure 14.** SEM-EDS image of the upper layer at 1873 K and 6 h: (a) SEM image; (b) #1 point scan; (c) #2 point scan; (d) #3 point scan; (e) Al element distribution; (f) O element distribution; (g) Mn element distribution; (h) Si element distribution.

Figure 14a shows the topography of the upper-layer material, which was mainly a gray material, mixed with a small amount of bright white material. Three points were selected for point scanning; the results are shown in Figure 14b–d. The compound at point 1 was  $\text{Al}_2\text{O}_3$ , and that at point 2 was  $\text{Mn}_5\text{Si}_3$ . The inclusions were  $\text{Al}_2\text{O}_3$  and  $\text{SiC}$ . The compound at point 3 was  $\text{SiC}$ , and a small amount of  $\text{Al}_2\text{O}_3$  was included, which was consistent with the previous XRD analysis results. Figure 14e–h shows the element distribution of the upper-layer material. The surface scan of the upper material showed the presence of highly overlapping Al and O elements, indicating that the upper-layer material mainly comprised  $\text{Al}_2\text{O}_3$ , with a small amount of  $\text{Mn}_5\text{Si}_3$  mixed in. This indicates that even under the optimal conditions, a small amount of  $\text{Mn}_5\text{Si}_3$  still entered the upper-layer material because when  $\text{LiAlSi}_2\text{O}_6$  formed  $\text{Mn}_5\text{Si}_3$ ,  $\text{Al}_2\text{O}_3$  was also decomposed, which caused a small amount of  $\text{Mn}_5\text{Si}_3$  to be carried into the upper layer by  $\text{Al}_2\text{O}_3$ . The mechanistic process of the reaction was shown in Figure 15.

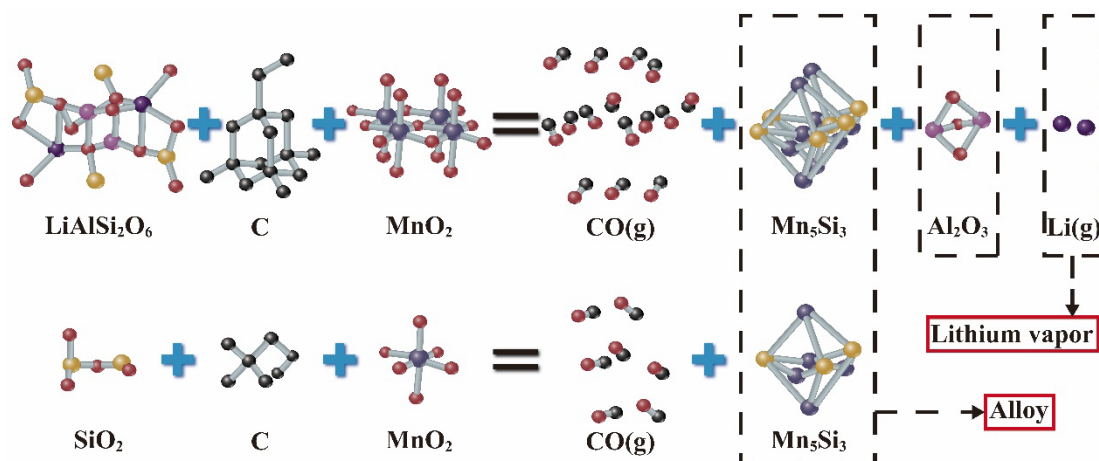


Figure 15. Reaction mechanism diagram.

#### 4. Conclusions

1. Thermodynamic calculations were carried out using HSC6.0 thermodynamic software. We found that  $\text{SiO}_2$  in the ore preferentially participated in the reaction compared with  $\text{LiAlSi}_2\text{O}_6$ . Compared with the reaction of  $\text{SiO}_2 + \text{C}$  and  $\text{LiAlSi}_2\text{O}_6 + \text{C}$ , the decrease was 651 K and 667 K, respectively, indicating that the addition of  $\text{MnO}_2$  reduced the reaction temperature and increased the feasibility of the reaction.
2. Due to the limited feed amount and the low lithium content in spodumene ore, it was difficult to collect the lithium condensate in a single step, so the lithium-rich condensate was collected through multiple experiments. The collected condensate contained 19.47% Li, which was 10.85 times more enriched compared with spodumene.
3. Reduction temperature and time were two important factors affecting the reaction. With increased temperature and time, spodumene ore was gradually reduced; when the reduction temperature was 1873 K and the reduction time was 6 h, the spodumene ore reaction was complete, the volatilization rate of lithium was 97.65%, and the direct yield of  $\text{Mn}_5\text{Si}_3$  was 86.47%.

**Author Contributions:** In this joint work, each author contributed according to their expertise and capability. Conceptualization, M.Y. and T.Q.; methodology, M.Y., K.Y., R.J., X.C., W.Z. and T.Q.; theoretical basis, M.Y. and K.Y.; formal analysis, M.Y.; investigation, X.C., R.J. and W.Z.; resources, T.Q.; data curation, M.Y. and T.Q.; writing—original draft preparation, M.Y.; writing—review and editing, M.Y.; visualization, K.Y.; supervision, T.Q.; project administration, T.Q.; funding acquisition, T.Q. All authors have read and agreed to the published version of the manuscript.

**Funding:** This research was funded by the Yunnan Provincial Academician Free Exploration Project (2022HA006).

**Data Availability Statement:** The data presented in this study are available upon request from the corresponding author. The data are not publicly available because related studies are ongoing.

**Conflicts of Interest:** The authors declare no conflict of interest. The funders had no role in the design of the study; in the collection, analyses, or interpretation of data; in the writing of the manuscript; or in the decision to publish the results.

#### References

1. Xie, R.; Zhu, Y.; Liu, J.; Li, Y. The flotation behavior and adsorption mechanism of a new cationic collector on the separation of spodumene from feldspar and quartz. *Sep. Purif. Technol.* **2021**, *264*, 118445. [CrossRef]
2. Lajoie-Leroux, F.; Dessemond, C.; Soucy, G.; Laroche, N.; Magnan, J.F. Impact of the impurities on lithium extraction from  $\beta$ -spodumene in the sulfuric acid process. *Miner. Eng.* **2018**, *129*, 1–8. [CrossRef]
3. Fosu, A.Y.; Kanari, N.; Vaughan, J.; Chagnes, A. Literature Review and Thermodynamic Modelling of Roasting Processes for Lithium Extraction from Spodumene. *Metals* **2020**, *10*, 1312. [CrossRef]

4. Xie, R.; Zhu, Y.; Liu, J.; Li, Y.; Wang, X.; Shumin, Z. Research Status of Spodumene Flotation: A Review. *Miner. Process. Extr. Metall. Rev.* **2020**, *42*, 321–334. [[CrossRef](#)]
5. Salakjani, N.K.; Singh, P.; Nikoloski, A.N. Acid roasting of spodumene: Microwave vs. conventional heating. *Miner. Eng.* **2019**, *138*, 161–167. [[CrossRef](#)]
6. Rosales, G.D.; Resentera, A.C.J.; Gonzalez, J.A.; Wuilloud, R.G.; Rodriguez, M.H. Efficient extraction of lithium from  $\beta$ -spodumene by direct roasting with NaF and leaching. *Chem. Eng. Res. Des.* **2019**, *150*, 320–326. [[CrossRef](#)]
7. Guo, H.; Kuang, G.; Wang, H.; Yu, H.; Zhao, X. Investigation of Enhanced Leaching of Lithium from  $\alpha$ -Spodumene Using Hydrofluoric and Sulfuric Acid. *Minerals* **2017**, *7*, 205. [[CrossRef](#)]
8. Fosú, A.Y.; Kanari, N.; Bartier, D.; Vaughan, J.; Chagnes, A. Novel extraction route of lithium from alpha-spodumene by dry chlorination. *RSC Adv.* **2022**, *12*, 21468–21481. [[CrossRef](#)]
9. Abdullah, A.A.; Oskierski, H.C.; Altarawneh, M.; Senanayake, G.; Lumpkin, G.; Dlugogorski, B.Z. Phase transformation mechanism of spodumene during its calcination. *Miner. Eng.* **2019**, *140*, 105883. [[CrossRef](#)]
10. Fosú, A.Y.; Kanari, N.; Bartier, D.; Hodge, H.; Vaughan, J.; Chagnes, A. Physico-Chemical Characteristics of Spodumene Concentrate and Its Thermal Transformations. *Materials* **2021**, *14*, 7423. [[CrossRef](#)]
11. Qiu, S.; Liu, C.; Yu, J. Conversion from  $\alpha$ -spodumene to intermediate product  $\text{Li}_2\text{SiO}_3$  by hydrothermal alkaline treatment in the lithium extraction process. *Miner. Eng.* **2022**, *183*, 107599. [[CrossRef](#)]
12. Guo, H.; Lv, M.; Kuang, G.; Wang, H. Enhanced lithium extraction from  $\alpha$ -spodumene with fluorine-based chemical method: A stepwise heat treatment for fluorine removal. *Miner. Eng.* **2021**, *174*, 107246. [[CrossRef](#)]
13. Rezaee, M.; Han, S.; Sagzhanov, D.; Vaziri Hassas, B.; Slawewski, T.M.; Agrawal, D.; Akbari, H.; Mensah-Biney, R. Microwave-assisted calcination of spodumene for efficient, low-cost and environmentally friendly extraction of lithium. *Powder Technol.* **2022**, *397*, 116992. [[CrossRef](#)]
14. Barbosa, L.I.; Valente, G.; Orosco, R.P.; González, J.A. Lithium extraction from  $\beta$ -spodumene through chlorination with chlorine gas. *Miner. Eng.* **2014**, *56*, 29–34. [[CrossRef](#)]
15. Chen, Y.; Tian, Q.; Chen, B.; Shi, X.; Liao, T. Preparation of lithium carbonate from spodumene by a sodium carbonate autoclave process. *Hydrometallurgy* **2011**, *109*, 43–46. [[CrossRef](#)]
16. Song, Y.; Zhao, T.; He, L.; Zhao, Z.; Liu, X. A promising approach for directly extracting lithium from  $\alpha$ -spodumene by alkaline digestion and precipitation as phosphate. *Hydrometallurgy* **2019**, *189*, 105141. [[CrossRef](#)]
17. Dessemmond, C.; Lajoie-Leroux, F.; Soucy, G.; Laroche, N.; Magnan, J.-F. Spodumene: The Lithium Market, Resources and Processes. *Minerals* **2019**, *9*, 334. [[CrossRef](#)]
18. Kuang, G.; Liu, Y.; Li, H.; Xing, S.; Li, F.; Guo, H. Extraction of lithium from  $\beta$ -spodumene using sodium sulfate solution. *Hydrometallurgy* **2018**, *177*, 49–56. [[CrossRef](#)]
19. Guo, H.; Yu, H.-Z.; Zhou, A.-A.; Lü, M.-H.; Wang, Q.; Kuang, G.; Wang, H.-D. Kinetics of leaching lithium from  $\alpha$ -spodumene in enhanced acid treatment using  $\text{HF}/\text{H}_2\text{SO}_4$  as medium. *Trans. Nonferrous Met. Soc. China* **2019**, *29*, 407–415. [[CrossRef](#)]
20. Grasso, M.L.; González, J.A.; Gennari, F.C. Lithium extraction from  $\beta$ - $\text{LiAlSi}_2\text{O}_6$  using  $\text{Na}_2\text{CO}_3$  through thermal reaction. *Miner. Eng.* **2022**, *176*, 107349. [[CrossRef](#)]
21. Rosales, G.D.; Resentera, A.C.J.; Wuilloud, R.G.; Rodriguez, M.H.; Esquivel, M.R. Optimization of combined mechanical activation-leaching parameters of low-grade  $\alpha$ -spodumene/NaF mixture using response surface methodology. *Miner. Eng.* **2022**, *184*, 107633. [[CrossRef](#)]
22. Salakjani, N.K.; Singh, P.; Nikoloski, A.N. Production of Lithium—A Literature Review. Part 2. Extraction from Spodumene. *Miner. Process. Extr. Metall. Rev.* **2019**, *42*, 268–283. [[CrossRef](#)]
23. Zhang, X.; Zeng, X.; Shan, Y.; Li, Z.; Zeng, Y.; Asselin, E. Solubility and Modeling of  $\text{Li}_2\text{SO}_4 \cdot \text{H}_2\text{O}$  in Aqueous  $\text{H}_2\text{SO}_4$ – $\text{MgSO}_4$  Solutions for Lithium Extraction from Spodumene. *J. Chem. Eng. Data* **2022**, *67*, 919–931. [[CrossRef](#)]
24. Wang, X.; Hu, H.; Liu, M.; Li, Y.; Tang, Y.; Zhuang, L.; Tian, B. Comprehensive utilization of waste residue from lithium extraction process of spodumene. *Miner. Eng.* **2021**, *170*, 06986. [[CrossRef](#)]
25. Meshram, P.; Pandey, B.D.; Mankhand, T.R. Extraction of lithium from primary and secondary sources by pre-treatment, leaching and separation: A comprehensive review. *Hydrometallurgy* **2014**, *150*, 192–208. [[CrossRef](#)]
26. Han, G.; Gu, D.; Lin, G.; Cui, Q.; Wang, H. Recovery of lithium from a synthetic solution using spodumene leach residue. *Hydrometallurgy* **2018**, *177*, 109–115. [[CrossRef](#)]
27. Kracek, F.C. The Binary System  $\text{Li}_2\text{O}$ – $\text{SiO}_2$ . *J. Phys. Chem.* **1930**, *34*, 2641–2650. [[CrossRef](#)]